LA-UR- 11-05320

Approved for public release; distribution is unlimited.

Title: The evolution of solid density within a thermal explosion II. Dynamic proton radiography of cracking and solid consumption by burning

Author(s): Laura Smilowitz, Bryan F. Henson, Jerry J. Romero, Blaine W Asay, Andy Saunders, Frank E. Merrill, Chris Morris, Kris Kwiatkowski, Gary P. Grim, Fassah Marriam, Cindy Schwartz, Gary Hogan, Paul Nedrow, Mathew Murray, Niel Thompson, Camilo Espinoza, Doug Lewis, Joe Bainbridge, Wendy McNeil, Mark Marr-Lyon and Paul Rightly

Intended for: Journal of Applied Physics

Los Alamos
NATIONAL LABORATORY
EST. 1943

Los Alamos National Laboratory, an affirmative action/equal opportunity employer, is operated by the Los Alamos National Security, LLC for the National Nuclear Security Administration of the U.S. Department of Energy under contract DE-AC52-06NA25396. By acceptance of this article, the publisher recognizes that the U.S. Government retains a nonexclusive, royalty-free license to publish or reproduce the published form of this contribution, or to allow others to do so, for U.S. Government purposes. Los Alamos National Laboratory requests that the publisher identify this article as work performed under the auspices of the U.S. Department of Energy. Los Alamos National Laboratory strongly supports academic freedom and a researcher's right to publish; as an institution, however, the Laboratory does not endorse the viewpoint of a publication or guarantee its technical correctness.

Form 836 (7/06)

The evolution of solid density within a thermal explosion II. Dynamic proton radiography of cracking and solid consumption by burning

L. Smilowitz, B. F. Henson, J. J. Romero, B. W. Asay, A. Saunders, F. E. Merrill, C. L. Morris, K. Kwiatkowski, G. Grim, F. Mariam, C. L. Schwartz, G. Hogan, P. Nedrow, M. M. Murray, T. N. Thompson, C. Espinoza, D. Lewis, J. Bainbridge, W. McNeil, P. Rightley, and M. Marr-Lyon

Los Alamos National Laboratory
Los Alamos, NM 87545

PACS numbers: 82.33.Vx; 25.40.Cm; 82.30.Lp; 82.40.-g

ABSTRACT

We report proton transmission images obtained subsequent to the laser assisted thermal ignition of a sample of PBX 9501 (a plastic bonded formulation of the explosive nitramine octahydro-1,3,5,7-tetranitro-1,3,5,7-tetrazocine (HMX)). We describe the laser assisted thermal ignition technique as a means to synchronize a non-linear thermal ignition event while preserving the subsequent post-ignition behavior. We have obtained dynamic proton transmission images at two spatial magnifications and viewing both the radial and transverse axis of a solid cylindrical sample encased in aluminum. Images have been obtained with 3 to 15 microsecond temporal resolution and approximately 100 μm spatial resolution at the higher magnification. We observe case expansion from very early in the experiment, until case fragmentation. We observe spatially anisotropic features in the transmission which we attribute to cracking in the solid explosive, in agreement with previous measurements conducted on two dimensional samples with optical viewing. Digital analysis of the images also reveals spatially isotropic features which we attribute to the evolution of the loss of density by burning subsequent to thermal ignition.

I. INTRODUCTION

Subsonic events in high explosives (HE) such as thermal explosion are inherently difficult to study.[1] Unlike a detonation, which can be initiated with very good precision, thermal explosion timing is spontaneous and notoriously difficult to predict. The duration of the direct heating that leads to a thermal explosion can span minutes to days,[2, 3] with final ignition and post-ignition burn propagation occurring in tens of microseconds. This final switch in time scales occurs at a time controlled by the HE itself, which is subject to a nonlinear positive feedback whereby exothermic reactions increase local temperature and accelerate temperature dependent reaction rates. Further complicating studies of subsonic thermal explosion is the fact that post-ignition burn propagation begins with sub-sonic velocities low enough that material and case conditions ahead of the reaction front can be communicated to the reaction front and influence it, another complication which is simplified in supersonic detonation. Experimentally, observing a thermal explosion with optical techniques such as fast framing cameras or spectroscopy are useful only until the case confinement is breached and light and smoke from the reaction obscure the diagnostics.

Despite the difficulties outlined, looking inside a thermal explosion is essential in order to understand the relevant phenomenology and to deconvolve the mechanisms which combine to control energy release. These questions ultimately must be addressed in order to be able to predict reaction violence of an HE system subjected to an abnormal thermal environment.

Based on the need to observe the transition to ignition and post-ignition burn propagation in a thermal explosion, we have worked out several technical problems to allow radiographic imaging of thermal explosions.[4] Radiography provides a measure of the evolution of density caused by material flow and decomposition leading up to ignition, as we have reported in a previous paper in this series,[5] and then a measure of the rapid consumption of material during burn propagation subsequent to ignition. We have designed a small scale radial thermal explosion experiment, utilizing cylindrical symmetry, enabling research scale experiments.[6] We have applied thermal boundary conditions that drive ignition to a single central point, giving up traditional one dimensionality in exchange for the ability to predetermine the ignition location.[2, 6, 7] A model of pre-ignition thermal decomposition for HMX based formulations has been refined to the point where we can predict an ignition time with tens of seconds accuracy.[8] Triggering techniques have been developed that enable us to synchronize the thermal ignition to a radiographic source within this few second.[4, 9]

We have fielded these thermal explosion experiments using two different types of radiography. We have collected multiple dynamic images of thermal explosion events using proton radiography at the Los Alamos National Laboratory Proton Radiography (pRad) facility,[4, 10] and, with Tringe et al., [11, 12] we have collected multiple dynamic x-ray images at the Lawrence Livermore National Laboratory Hydra Facility.

In this paper, we present proton radiographic images for thermal explosions using the HMX (octahydro-1,3,5,7-tetranitro-1,3,5,7-tetrazocine) based formulations PBX 9501 (95 wt% HMX, 2.5 wt% nitroplasticizer, and 2.5 wt% estane, initial density 1.83 g/cc. Two different cylindrical aspect ratios have been investigated and two different case configurations, differing in endcap

thickness, have been used. We will describe the burn propagation behavior for PBX 9501 as well as compare different geometries and case confinement strengths. Analysis of the radiographic images obtained will be discussed. We will conclude by describing the understanding of ignition and subsequent sub-sonic burn propagation enabled by this data set.

II. EXPERIMENT

The radial thermal explosion experiment is designed to be a small scale, reproducible experiment with a controlled ignition location and a case made of low atomic number materials to be compatible with radiographic imaging.[6] For these experiments, a case of 1/8" thick aluminum is found to provide sufficient confinement at low enough areal density (the density integrated along the proton beam axis) to allow for both prompt burning and consumption of the HMX after ignition and radiographic imaging with sufficient signal to noise.[4, 7]

Two schematics of the experimental design used in these experiments are shown in Fig. 1. The assembly is composed of two half cylinders, each containing a cylindrical sample of HE encased in the cylindrical confinement and an endcap piece used for combining the halves together. The full cylinder is bound by a glue seal at the midplane and strengthened by bolts in the endcaps. All configurations discussed in this paper utilized 1/8" cylindrical wall thickness. Two different endcap thicknesses were used, 1/8" and 1/16", as will be indicated later. Our intial design was based on a ½" diameter, 2:1 aspect ratio cylinder, as shown in Fig. 1 top. Subsequently we showed that a larger diameter was required in order to observe burning and HMX consumption for a longer period of time before the cylinder wall was reached by the

convective front, leading to a 1:1 aspect ratio design, shown in Fig. 1 bottom.

Thermal boundary conditions were applied such that ignition occurred at the center of the cylinder radially, and displaced approximately 1 mm from the center plane axially.[5, 6] We instrumented this midplane with internal thermocouples and fiber optics for the control and synchronization of triggering to be discussed below.[7, 9] A typical midplane instrumentation suite is shown in Fig. 2.

The typical temperature trajectory applied involved heating the cylindrical wall to 205 C over approximately one hour with hold points at 70 C and 178 C and heating rates of 5 C/min.[5] This trajectory allows the HE to equilibrate and the final 205 C boundary temperature allows the HE to self heat and develop a temperature gradient with the hottest point near the center of the cylinder.[7]

Thermal explosion experiments span time scales from the thousands of seconds laboratory time scale for the pre-ignition heat trajectory, to the acceleratory self heating and thermal runaway region lasting tens of seconds and creating internal heating rates of tens of degrees per minute, to the ignition regime and post-ignition burn propagation regime which take tens of microseconds for this scale of experiment. In order to capture observables spanning hours to microseconds, we developed triggering systems that indicate when that switch in time scales occurs. We have found that the internal thermocouples used to monitor self-heating can be used as a reliable trigger early enough in the breakout of ignition to trigger post-ignition diagnostics. We believe this trigger indicates the appearance of a charged plasma and thus likely represents the onset of gas phase combustion. A typical measurement made using a thermocouple placed close to the ignition volume is shown in Fig. 3.[2] A break-foil is used on the outside of the case as

a timing fiducial for when the case comes apart, which we approximate as the end of useful data acquisition as the confinement has been fully lost by this point.

In some cases, such as found at the pRad facility, being able to simply trigger external diagnostics when a thermal explosion event began was not enough. This facility is driven by an 800 MeV proton accelerator which delivers a 1 ms proton window every 50 ms, meaning that in order to capture a thermal explosion event, ignition needed to be synchronized to proton availability. In order to do this, we developed a synchronization technique that would allow us to accelerate the thermal explosion sequence without drastically altering the subsequent combustion process.[9] This technique involved using a fiber optic coupled to a free running Nd:YAG laser to provide a 150 μs temperature jump during the thermal runaway portion of the experiment. The laser pulse measured on a second fiber optic and the temperature rise caused by the laser pulse are shown in Fig. 4. What is observable from the internal thermocouples is that the laser provides a temperature jump which accelerates ignition to within a few hundred microseconds. The ignition event triggers the oscilloscope at time zero and the external breakfoil records case failure approximately 30 μs later for the ½" diameter experiment and 60 μs for the 1" diameter. We have conducted a series of experiments varying the laser pulse energy and mapped out the ignition delay as a function of pulse energy. Details of the laser synchronization technique have been published elsewhere.[2, 9]

Using these triggering and synchronization techniques, we have now run a series of experiments at both the pRad[4] and Hydra x-ray facilities.[12] In these experiments, we have compared effects of scaling, shot size, formulation, case confinement, and synchronization.

III. Results: PBX 9501

A. The Response of PBX 9501

We now have 16 dynamic experiments that have been conducted at the pRad facility. The overall behavior we observe in the resulting images is that subsequent to ignition, indicated by the internal trigger thermocouple, endcap deformation induces a state of axial tension in the solid, resulting in crack propagation within ~ 10-20 μs at velocities from 300 to greater than 800 m/s depending upon endcap thickness. Such cracking has been observed previously by optical techniques in quasi two-dimensional experiments.[13] The cracks propagate and expand to the case boundary, but do not consume a large fraction of the HE. A wave marking the onset of significant solid consumption is also launched within 10-20 μs of ignition. The wavefront travels at 150 to 250 m/s, independent of wall thickness or crack velocity, and faster along the cylinder axis than radially. We interpret this front as a wave of convective burning, permeating the porous solid and igniting the surface. Following this for another ~50 μs is the slower loss of HE density as solid is consumed by conductive burning.

B. Radiography

A successful radiographic experiment requires synchronization of ignition with the availability of protons and material confinement both transmissive to proton illumination and of sufficient strength to enable pressurization and the observation of burning. Another variable is the confinement of gas phase products. The midplane seal is sufficient to allow pressurization throughout the heating of the sample, which is crucial to a reproducible pre-ignition boundary

condition and thus reproducible time to ignition. The strength of the seal and bolt pattern are also such that the midplane opens along the cylinder axis at approximately the same time that internal thermocouple signals indicate the beginning of gas phase burning. This is also a crucial timing issue as the proton image contrast is dependent on removing high pressure gas phase products so that the resulting transmission change is dependent primarily on the evolution of the solid areal density. This results in a moving case edge which must be considered when interpreting side view experiments even at early times, but does not affect the radial view until much later, when convection reaches the cylinder wall and significant deformation orthogonal to the cylinder axis is observed. These effects will be noted as they are apparent in the images.

In the next two sections direct transmission images are shown, as they most clearly indicate the overall response during the experiment. This will be followed by more refined analysis, including image normalization, which will better reveal the fine resolution features, such as cracking and consumption, that are contained in the data.

1. Side View

Four frames from an experiment using a ½" diameter 2:1 aspect ratio sample are shown in Figure 5. Case confinement of 1/8" cylinder and endcap walls were used. The spatial resolution of these proton transmission images is approximately 70 μm. The grey scale in Fig. 5 uses white to represent high transmission (T=1) and black to represent low transmission (T=0). The endcaps are the black vertical bands and the vertical light line at the center is the midplane of the shot. The orientation of these images is rotated 90 degrees from Fig 1 (bottom). The windings

apparent in this experiment are due to the nichrome heater applied to the boundary in early experiments. A new design based on kapton heaters was used in all subsequent experiments. The times in each frame are relative to the internal thermocouple signal and indicate the onset of gas phase combustion. The opening of the midplane along the cylinder axis is apparent in the 26 and 40 μs frames. The escape of product gases from the midplane is also observed as the hemisphere emerging from the midplane, outside the cylinder edge, particularly in the 26 μs frame. Frames 54 and 61 μs show very high deformation later in the experiment.

Five frames from an experiment using a 1" diameter 1:1 aspect ratio sample are shown in Figure 6. Case confinement of 1/8" cylinder and endcap walls were used. The interframe time as 20 μs. The spatial resolution and transmission scale are the same as for Fig. 5. The orientation of these images is rotated 90 degrees from Fig. 1 (bottom). The general features of midplane opening, product gas escape and deformation are the same as for Fig. 5, however internal burning proceeds for much longer before a cylinder wall is reached by convective burning. This is a significant advantage during analysis and interpretation and is the reason that all subsequent experiments use this diameter and aspect ratio.

Five frames from an experiment using a 1" diameter 1:1 aspect ratio sample are shown in Figure 7. Case confinement of 1/8" cylinder and 1/16" endcap walls were used. The spatial resolution and transmission scale are the same as for Fig. 5. The orientation of these images is rotated 90 degrees from Fig 1 (bottom). The first frame shown is taken 12 μs after the thermocouple trigger. By this time, the endcaps are already visibly bowing, the center line has opened, and there is density loss and cracking visible in the HE. Frames were taken at 10 microsecond intervals. By the 40 μs frame, the endcaps have been punched out and the center

aluminum plugs are flying outward. These plugs are typical of these shots and their velocities have been measured to be ~800 m/s. [12]

2. *Radial View*

Three frames from an experiment using a 1" diameter 1:1 aspect ratio sample are shown in Figure 8. Case confinement of 1/8" cylinder and endcap walls were used. The interframe time was 20 μs. The spatial resolution and transmission scale are the same as for Fig. 5. The primary observations from this view have been the crack patterns, the radially symmetric increase in transmission over time and radial wall motion observed in the images.

3. *X-ray Radiography*

The proton transmission radiography requires laser synchronization in order to be able to capture dynamic images of thermal explosion during the less than 100% duty cycle of the proton accelerator. A sequence of four x-ray transmission images has been collected at the LLNL Hydra facility without requiring synchronization of the thermal explosion to the x-ray sources. This allowed verification that the laser synchronization technique did not significantly alter the outcome of the thermal explosion event. The experiment was the result of a Los Alamos Lawrence Livermore collaboration and details of the radial thermal explosion radiographed with four independent axis pulsed x-ray units was presented by Tringe et al. at the 14th International Symposium on Detonation.[12, 14] The behavior observed is similar to that observed with laser synchronized proton radiography. The velocity interpolated from the three radial views is approximately 300 m/s, in agreement with that measured in the laser synchronized pRad experiments. [12]

C. Image Analysis

We will discuss two forms of analysis with which to turn the radiographic images into digitized data. In the first we apply normalization techniques to elicit finely detailed changes in transmission during dynamic events by taking a ratio of the dynamic to a prior static image. In the second we perform various integrations of the transmission to obtain one dimensional line profiles of transmission that may be compared to calculated synthetic profiles.

We will then present a compilation of velocities in these experiments obtained by measuring the position of various features in the images, crack patterns, case opening, and the onset of density loss that we attribute to the initial propagation of combustion by convection, all as a function of frame time.

1. Normalization

The change in proton transmission shown in Fig. 9 was obtained by dividing the image second from the top of Fig. 7 by a static image obtained a few minutes before the laser synchronization of thermal ignition. Taking the ratio of these two images allows enhancement of details of the change between these two images. It is similar to displaying the transmission image in logarithmic scale, or flattening the dynamic range of the image in order to bring out small changes in transmission. Presenting images as ratios of images taken before and during a thermal explosion event works well for small changes. The bright and dark bands in the image, particularly at the edge of the endcap and midplane are caused by motions of high contrast steps. A small displacement of a high contrast edge creates a large difference. What is clearly visible in

this image ratio is the density change in the HE which appears as a random network of white that looks like cracks propagating to the endcap.

2. *Integration of transmission profiles*

Quantitative data is extracted from these images by drawing line profiles at various locations in the image and comparing these profiles at different image times. Fig. 10 shows an example of direct transmission image with actual calculated line profile superimposed. The peak at the midplane is where the case has begun to open and the transmission is approximately 0.9 where 1.0 represents the transmission through air. The fact that the transmission at the midplane is not 1.0 indicates high density gas and solid products are present. In fact, some of the products can be seen in the image. The transmission curve drops to about 0.25 in the aluminum endcap region. In the region between the midplane and endcaps, a plateau is observed with a slight gradient away from the midplane. This is due to the loss of HE density beginning at the midplane and then propagating towards the endcap. In subsequent frames, this density loss evolves. Another detail captured by the transmission profile is the fact that the transmission post-ignition is no longer flat, but has oscillations on it. These oscillations can be seen to correspond to spatial heterogeneities visible in the transmission images. They are not merely noise on a flat image, but represent a real phenomenon in the burn propagation; crack formation. The amplitude of the oscillation is a measure of the density loss in the crack.

3. *Velocities*

By taking transmission line profiles in the same spatial location from frames collected at different times relative to the thermocouple ignition trigger, a time sequence can be created.

Line profiles of the transmission ratio data from the experiment of Fig. 7 from eight frames taken between time 0 and time 80 microseconds are shown in Fig. 11. Horizontal lines representing the proton transmission through air and through the initial density of HE and aluminum case are included for comparison. The dashed line which is relatively flat at the initial HE/Al density is the line profile taken from an image prior to the onset of ignition. These profiles show the opening of the midplane, loss of HE density, and cracking in the HE (observable as oscillations in transmission). By plotting the approximate position of the leading edge of the transmission rise and of the later rise associated with the case separating along the cylinder axis, velocities can be determined. We have performed such analysis on many experiments to date and determined typical axial convective velocities to be on the order of 200 to 250 m/s. Due to the added complexity of the midplane opening, axial velocities are particularly difficult to interpret without simulation, and we will therefore describe the determination of these values in more detail in a third companion paper on the simulation of these results.[15] Radial velocities are more easily determined without the obscuring effects of the midplane at early times, and are therefore measured with better precision. An example of this is shown in Fig. 12, where integrations of the increase in the areal density, obtained from the measured transmission increase as a function of time,[5] are shown. In this figure a three point velocity of 166+/-2 m/s is indicated. We have applied similar analysis to a number of experiments where radial views have been obtained. A compilation of position as a function of time from several experiments are shown in Fig. 13, with midplane opening, viewed side on, plotted in Fig. 13c and radial position of the convective front as a function of time shown in Fig. 13b.

Velocities may also be determined, more subjectively, by tracking features in the images. This is particularly the case for the measurement of crack velocities. It is important to remember

that experimental signal to noise may determine where the observable edge appears, yielding only a lower bound velocity to single point measurements, however interframe progress should be less affected, if consistent features are tracked, yielding a more reliable velocity. Two sets of three images where the leading edge of the crack field is measured as a function of time are shown in Fig. 14. Time increases to the right by 10 μs per frame in the top three frames and 20 μs per frame in the bottom three. The solid black lines are guides to the eye. Using the radius drawn for each image and the interframe time linear regression yields velocities of 300+/-32 m/s in the top series and 350+/-29 m/s in the lower, just consistent within the error.

The same analysis is performed on an experiment conducted in the side view and is shown in Fig. 15. This experiment was nominally identical to those of Fig. 14 in mechanical confinement, in particular using the same endcap thickness, 1/8", and the same 20 μs interframe time as the lower set of radial images in Fig. 14. Again using the diameter and frame time we fit a crack velocity of 300 +/-32 m/s.

The position and time determined from these images is also compiled in Fig.13a. While the crack patterns do exhibit a remarkably symmetric structure, enforcing a circular averaging introduces error in excess of the simple regression error. Nevertheless, it is encouraging to achieve such reproducibility in these measurements, given the small number of experiments possible with accelerator based radiography. The ability to inter-compare different experiments enables significantly greater confidence in the conclusions we draw from these data.

Finally, another experiment conducted in the side view and is shown in Fig. 16. This experiment was different from those of Figs. 14 and 15 in the mechanical confinement, using a reduced endcap thickness of 1/16", and a 10 μs interframe time. Linear regression is problematic

as the velocity is clearly much faster, with cracks nearly reaching the endcap in the first image, and exhibiting a very nonlinear deceleration after the 30 μs, likely due to encountering the metal boundary. This is shown in Fig. 13a. A highly uncertain three point velocity of 550 m/s is indicated at early time by the open data points.

D. Preliminary Deflagration Model

Material in a thermal explosion is believed to be consumed by deflagration. Deflagration is the overall manner by which several sub-sonic processes combine to consume the material and release energy by burning. Such processes include thermal damage and cracking, which expose material surface, conductive burning, the relatively slow (0.001 to 1 m/s) process by which solid is consumed and convective burning, where burning proceeds much faster (100 to 1000 m/s) through the gas phase by convection, and can ignite conductive burning on the exposed surface. The assertion that an explosion is driven by deflagration and adequately described by the component processes described above had remained an unproven hypothesis until this work, as there had been no means of directly observing these processes as they combine to consume solid and release energy. A principle product of this work is the attempt to verify that this hypothesis is essentially correct, and that with these new radiographic techniques we now have the tools to deconvolve the individual contribution of each mechanism to the overall deflagration behavior.

1. The role of cracking

The observation of cracking is clearly demonstrated in Figs. 14-16, however the role of cracking in these experiments remains uncertain. A significantly higher crack velocity is observed for the case configuration using a thinner endcap, as is shown in the normalized image

in Fig. 16. This frame is the first dynamic frame obtained after the internal thermocouple trigger and the cracking pattern has nearly reached the endcap. The velocity of crack propagation is therefore a very sensitive function of the confinement, early deformation and the subsequent state of axial tension applied to the solid explosive early in the dynamic event. A preliminary determination of the convective velocity in the thin endcap experiment in Fig. 16 does not indicate a significantly different velocity from other side view experiments with thick confinement and slower crack velocity. We will present a fuller analysis of these convective velocities in the third paper in this series,[15] but we maintain a current hypothesis that in this particular experiment, one in which extensive material damage has been done to the PBX 9501 due to passage through the $\beta-\delta$ phase transformation, the convective velocity is independent of the dynamic cracking that is simultaneously occurring.

2. *Gaseous flame propagation by convection*

A symmetric isotropic increase in proton transmission (decrease in density) can also be seen, superimposed on these crack patterns, from numerical analysis of the images. This is shown in Fig. 12 where the radial transmission intensity is plotted as a function of a ½" diameter radial view.

Our interpretation of this symmetric structure is the propagation of a burn front. The few hundred m/s velocity implies that the burn front travels by convection through the gas phase and consumes only a few percent of the solid. This suggests a mechanism based on one dimensional convective[16] and conductive[17] burning in HMX. In this mechanism of internal, radially divergent burning, a propagating convective front ignites the solid, which is then consumed by a conductive burn.

3. Conductive burning and solid consumption

Conductive burning is the actual consumption of solid by burning. The rate of regression of the burning surface is determined by the surface temperature, which is a function of the distance of the flame from the surface. This distance is itself a function of pressure, therefore the rate of regression is an indirect function of the pressure. One dimensional linear regression as a function of pressure is relatively well understood and measured in a number of energetic materials, including HMX.

IV. CONCLUSIONS

In this work we have demonstrated the ability to radiograph thermal explosions, both using laser synchronized experiments at the LANL proton radiography facility, and using auto-ignition experiments at the LLNL Hydra multi-head x-ray facility. The utility of radiographic observables is their ability to provide a view inside a thermal explosion. From these experiments, we have been able to understand the mechanism of a thermal explosion and have put together a model capturing both the gas phase convective and solid state conductive components of a deflagration wave. Several parameters have been investigated including scaling the size of the HE and changing case confinement strength. We are currently beginning a series of longer aspect ratio experiments with the potential to undergo a deflagration to detonation transition.

V. ACKNOWLEDGEMENTS

This research was supported by Science Campaigns 1 and 2 and the Surety Program administered by Los Alamos National Laboratory, as well as the Joint Munitions Program administered by both the Departments of Energy and Defense.

VI. References

1. B. W. Asay, in *Shock Wave Science and Technology Reference Library*, edited by Y. Hori (Springer-Verlag, Berlin, 2009), Vol. 5, pp. 617.
2. L. Smilowitz, B. F. Henson, M. M. Sandstrom, B. W. Asay, D. M. Oschwald, J. J. Romero and A. M. Novak, AIP Conference Proceedings **845** (1), 1211-1214 (2006).
3. J. J. Yoh, M. A. McClelland, J. L. Maienschein, A. L. Nichols and C. M. Tarver, Journal of Applied Physics **100** (7), 073515 (2006).
4. L. Smilowitz, B. F. Henson, J. J. Romero, B. W. Asay, C. L. Schwartz, A. Saunders, F. E. Merrill, C. L. Morris, K. Kwiatkowski, G. Hogan, P. Nedrow, M. M. Murray, T. N. Thompson, W. McNeil, P. Rightley and M. Marr-Lyon, Physical Review Letters **100** (22), 228301-228304 (2008).
5. L. Smilowitz, B. F. Henson, J. J. Romero, B. W. Asay, A. Saunders, F. E. Merrill, C. L. Morris, K. Kwiatkowski, G. Grim, F. Mariam, C. L. Schwartz, G. Hogan, P. Nedrow, M. M. Murray, T. N. Thompson, C. Espinoza, D. Lewis, J. Bainbridge, W. McNeil, P. Rightley and M. Marr-Lyon, Journal of Applied Physics **submitted** (2011).
6. L. Smilowitz, B. F. Henson, M. M. Sandstrom, B. W. Asay and J. Romero, Thirteenth Symposium (International) on Detonation, 1026-1034 (2006).
7. L. Smilowitz, B. F. Henson, J. J. Romero, M. M. Sandstrom, B. W. Asay, C. Schwartz, A. Saunders, F. Merrill, C. Morris, M. M. Murray, W. V. McNeil, M. Marr-Lyon, P. M. Rightley and C. pRad, AIP Conference Proceedings **955**, 1139-1142 (2007).
8. B. F. Henson, L. Smilowitz, J. J. Romero and B. W. Asay, AIP Conference Proceedings **1195**, 257-262 (2009).
9. L. Smilowitz, B. F. Henson, M. M. Sandstrom, J. J. Romero and B. W. Asay, Applied Physics Letters **90** (24) (2007).
10. C. T. Mottershead and J. D. Zumbro, Proceedings of the IEEE Particle Accelerator Conference **2**, 1397-1399 (1998).
11. P. C. Souers, H. G. Andreski, J. Batteux, B. Bratton, C. Cabacungan, C. F. Cook Iii, S. Fletcher, R. Garza, D. Grimsley, J. Handly, A. Hernandez, P. McMaster, J. D. Molitoris, R. Palmer, J. Prindiville, J. Rodriguez, D. Schneberk, B. Wong and P. Vitello, Propellants, Explosives, Pyrotechnics **31** (2), 89-97 (2006).
12. J. W. Tringe, J. D. Molitoris, L. Smilowitz, J. R. Kercher, H. K. Springer, B. F. Henson, E. A. Glascoe, D. W. Greenwood, R. G. Garza, B. M. Wong, J. D. Batteux and J. L. Maienschein, AIP Conference Proceedings **1195**, 424-427 (2009).
13. P. M. Dickson, B. W. Asay, B. F. Henson and L. B. Smilowitz, Proceedings of the Royal Society of London Series A-Mathematical Physical and Engineering Sciences **460** (2052), 3447-3455 (2004).
14. J. W. Tringe, E. A. Glascoe, J. R. Kercher, T. M. Willey, H. K. Springer, D. W. Greenwood, J. D. Molitoris, L. Smilowitz, B. F. Henson and J. L. Maienschein, presented at the Fourteenth Symposium (International) on Detonation, Coeur d'Alene, ID, 2010 (unpublished).
15. B. F. Henson, L. B. Smilowitz, A. Saunders, F. E. Merrill, C. L. Morris and C. L. Schwartz, Journal of Applied Physics **to be submitted** (2011).
16. T. L. Boggs, Prog Astronaut Aeronaut **90**, 121-175 (1984).

17. J. L. Maienschein, J. F. Wardell, M. R. DeHaven and C. K. Black, Propellants, Explosives, Pyrotechnics **29** (5), 287-295 (2004).

Figure Captions

Fig. 1: Radial thermal explosion experiment schematics. White region is HE, grey is aluminum case, dark grey shows steel screws. Top: Initial 2:1 aspect ratio design. Bottom: 1:1 aspect ratio design.

Fig. 2: View of the cylinder midplane bisecting the experiment along the cylinder axis. Six 75 μm wire thermocouples and two larger, 200 μm optical fibers are shown. The metal ring is the case wall and the white material is the explosive PBX 9501.

Fig. 3: Thermocouple trigger technique. Solid line is thermocouple direct voltage output (converted to ^{o}C). Dashed line is breakfoil signal.

Fig. 4: Laser synchronization. The black curve is the central temperature during laser illumination and ignition, measured by 75 μm bead chromel/alumel alloy (type K) thermocouple. The solid grey line is the fiber signal measured by an InGas photodiode, illustrating the laser pulse shape and relative intensity profile.

Fig. 5: Proton transmission images of the lower half of a 1/2" diameter, 2:1 aspect ratio experiment imaged in side view. Case confinement of 1/8" cylinder and endcap walls were used. Frames times are relative to the rise of the internal trigger thermocouple.

Fig. 6: Proton transmission images of 1" diameter, 1:1 aspect ratio experiment imaged in side view. Case confinement of 1/8" cylinder and endcap walls were used. The time sequence begins from the top with an interframe time of 20 μs.

Fig. 7: Proton transmission images of 1" diameter, 1:1 aspect ratio experiment imaged in side view. Case confinement of 1/8" cylinder and 1/16" endcap walls were used. The time sequence starts at the top 12 μs after the rise of the internal thermocouple and the interframe time is 10 μs.

Fig. 8: Proton transmission images of 1" diameter, 1:1 aspect ratio experiment imaged in radial view. Case confinement of 1/8" cylinder and 1/8" endcap walls were used. The time sequence begins from the top with an interframe time of 20 μs.

Fig. 9: Ratio of the image second from the top in Fig. 7 divided by a static image taken several minutes before ignition.

Fig. 10: Integrated line profile 2 mm wide down the center of the cylinder axis obtained by integration of the transmission ratio shown in Fig. 9. The line profile is overlayed on the absolute transmission image second from the top of Fig. 7.

Fig. 11: Line profiles for times from 12 to 92 μs after the ignition trigger obtained from transmission ratios generated in the experiment shown in Fig. 7. Horizontal lines show transmission for air and initial HE/Al. The bold, bottom line is the profile from the pre-ignition static image.

Fig. 12: Integrated transmission line profiles that have been converted to areal density for a ½" diameter experiment in the radial view. The areal density is plotted as a function of radius. The dashed lines are guides to the eye indicating the position of the convective front. The interframe time was 15 μs.

Fig. 13: Position as a function of frame time for three different features in a number of experiments. a) location of the leading edge of crack patterns bounded by the black circles in Figs. 14 – 16, b) location of the leading edge of convection, bounded by the dashed semi-circle in Fig. 12, c) location of case edges as they are observed to open in the side view.

Fig. 14: Two 1" diameter experiments imaged in the radial view. 1/8" wall and endcap thickness was used in both experiments. The images are transmission ratios and the black circles are guides to the eye, bounding the pattern of cracking and denoting the leading resolvable edge. Time proceeds from left to right, with a 10 μs interframe time in the top experiment and 20 μs in the bottom.

Fig. 15: A 1" diameter experiment imaged in the sideview. 1/8" wall and endcap thickness was used in this experiment. The images are transmission ratios and the black circles are guides to the eye, bounding the pattern of cracking and denoting the leading resolvable edge. Time proceeds from left to right, with a 20 μs interframe time.

Fig. 16: A 1" diameter experiment imaged in the sideview. 1/8" wall and 1/16" endcap thicknesses were used in this experiment. The images are transmission ratios and the black circles are guides to the eye, bounding the pattern of cracking and denoting the leading resolvable edge. Time proceeds from left to right, with a 10 μs interframe time.

Figures

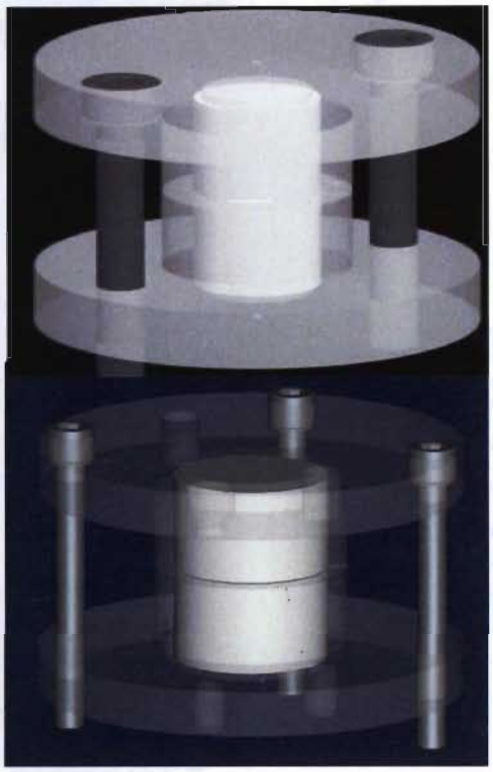

Figure 1: Smilowitz et al.

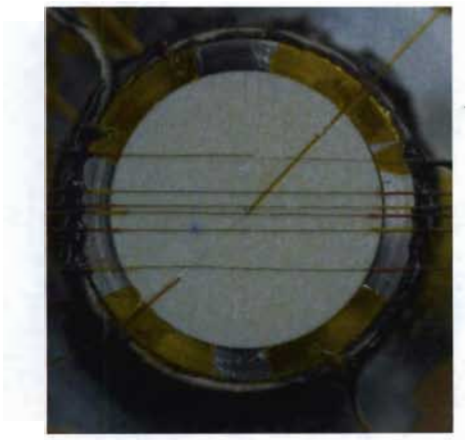

Figure 2: Smilowitz et al.

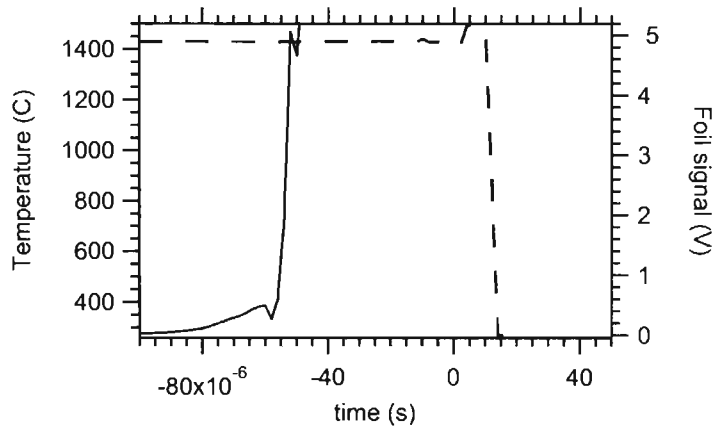

Figure 3: Smilowitz et al.

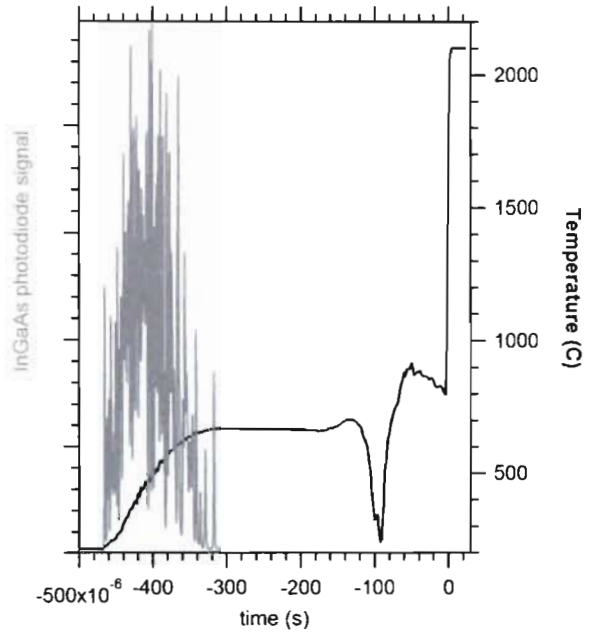

Figure 4: Smilowitz et al.

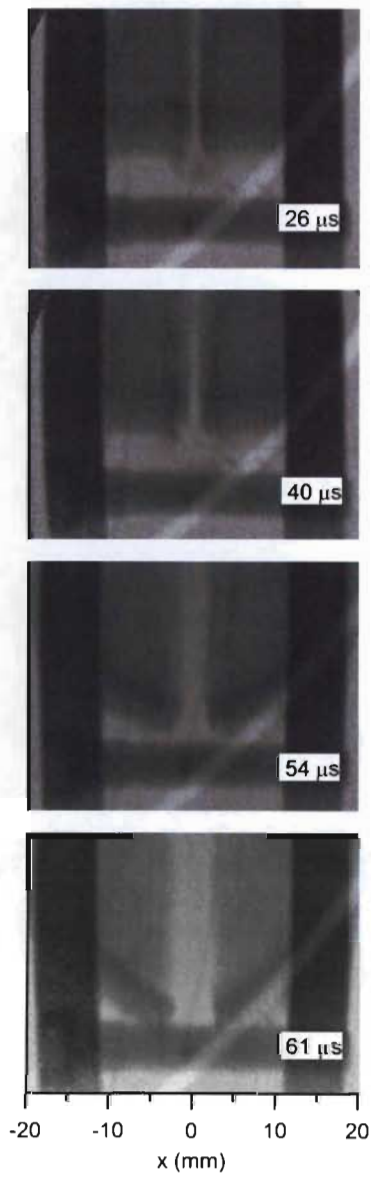

Figure 5: Smilowitz et al.

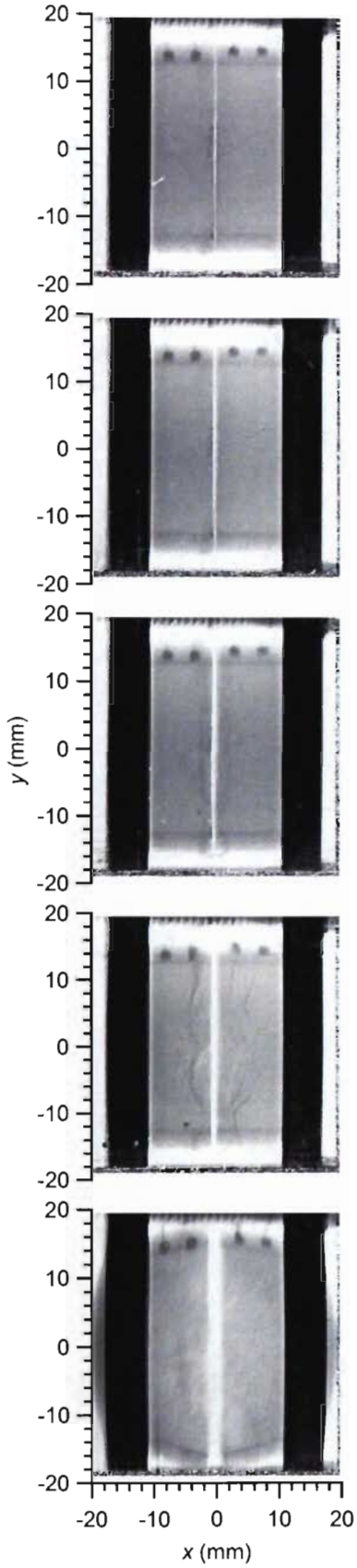

Figure 6: Smilowitz et al.

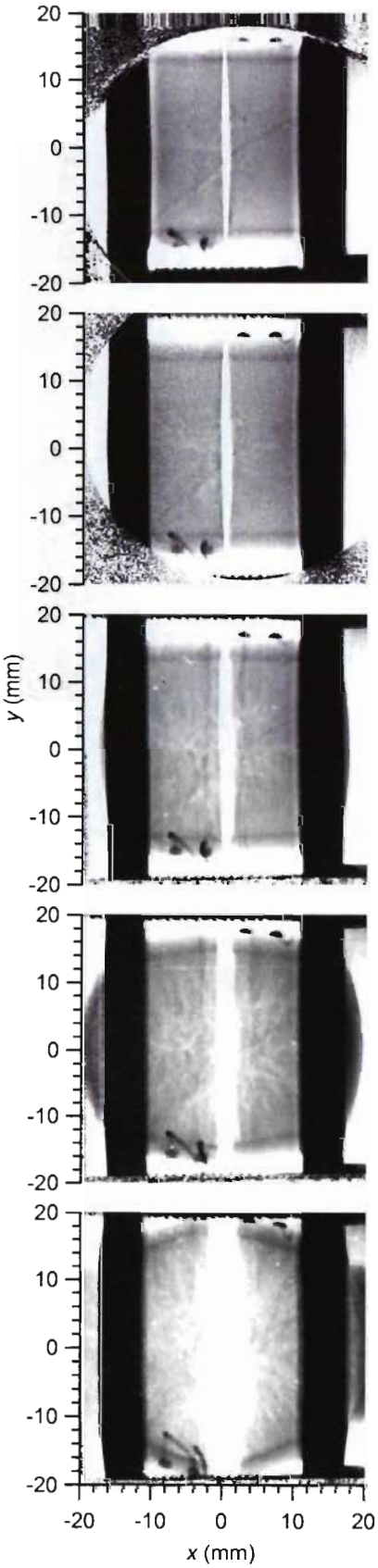

Figure 7: Smilowitz et al.

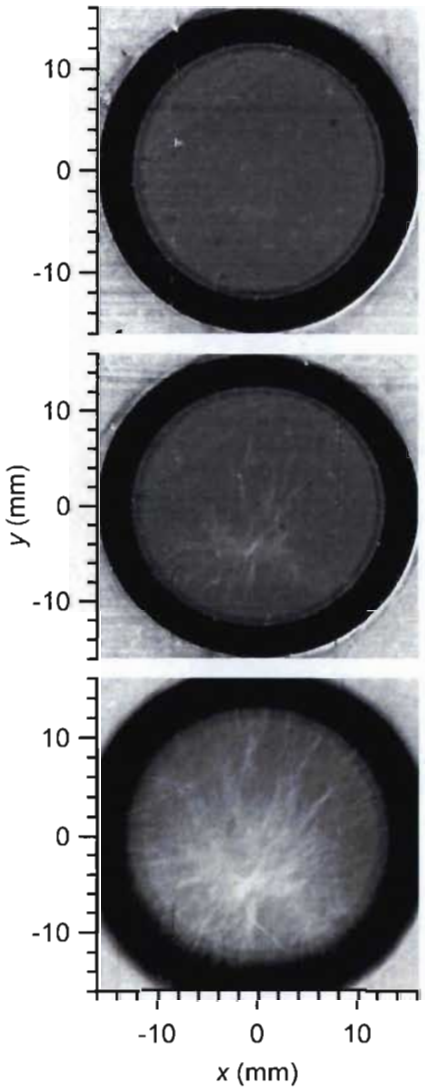

Figure 8: Smilowitz et al.

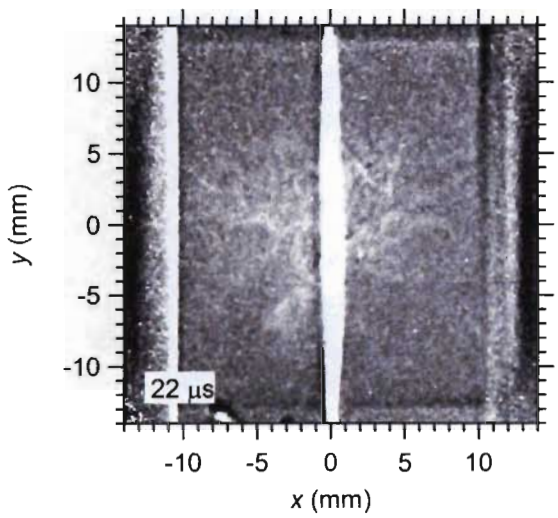

Figure 9: Smilowitz et al.

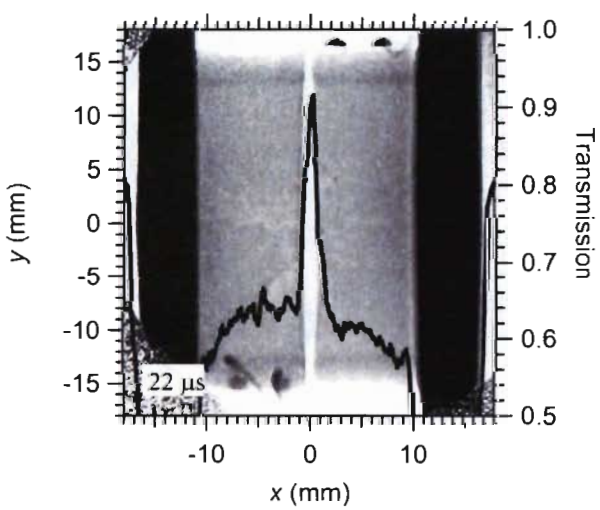

Figure 10: Smilowitz et al.

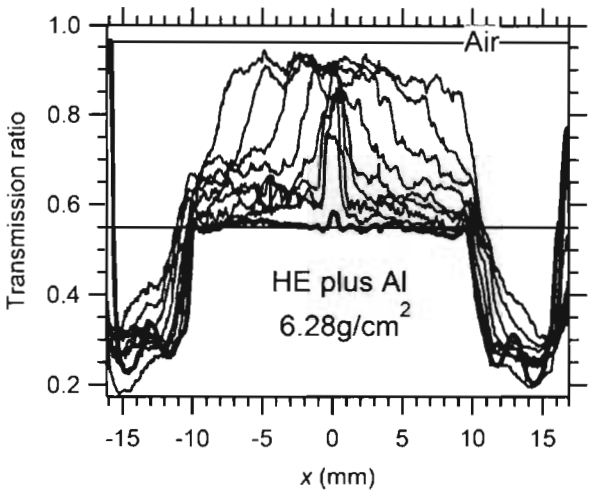

Figure 11: Smilowitz et al.

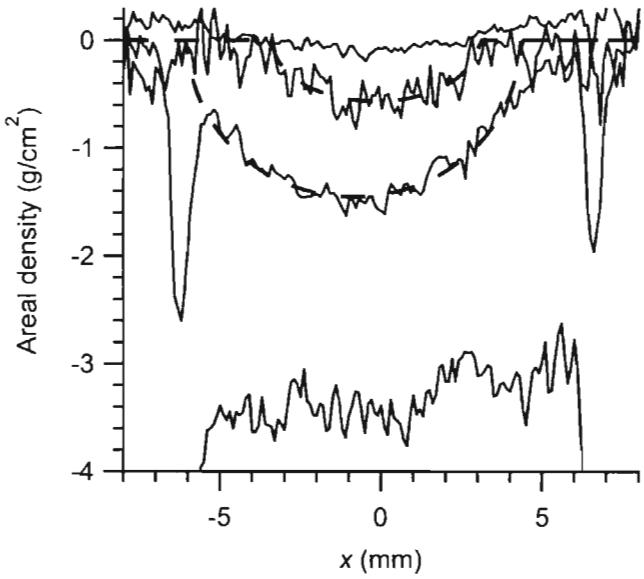

Figure 12: Smilowitz et al.

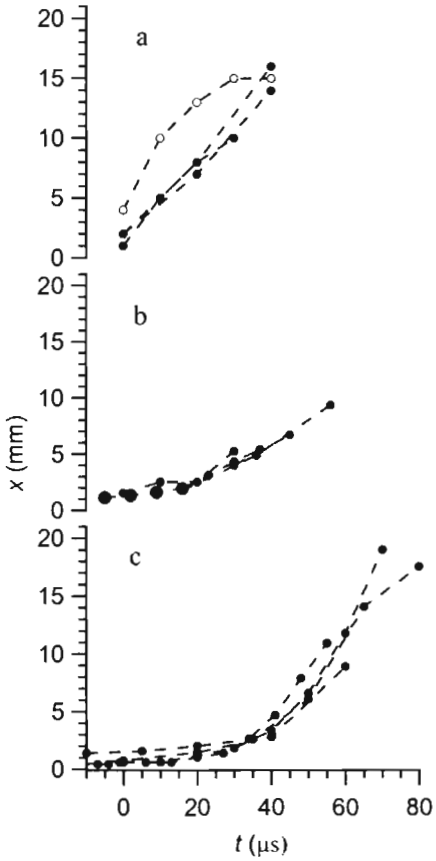

Figure 13: Smilowitz et al.

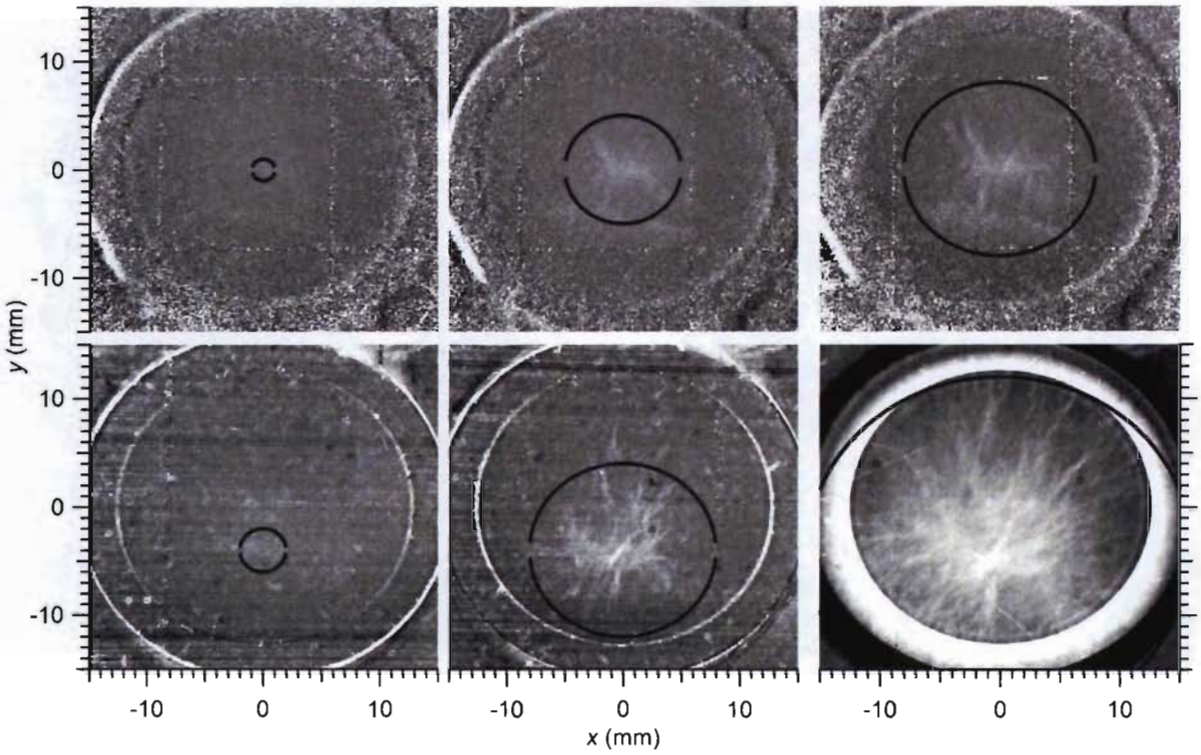

Figure 14: Smilowitz et al.

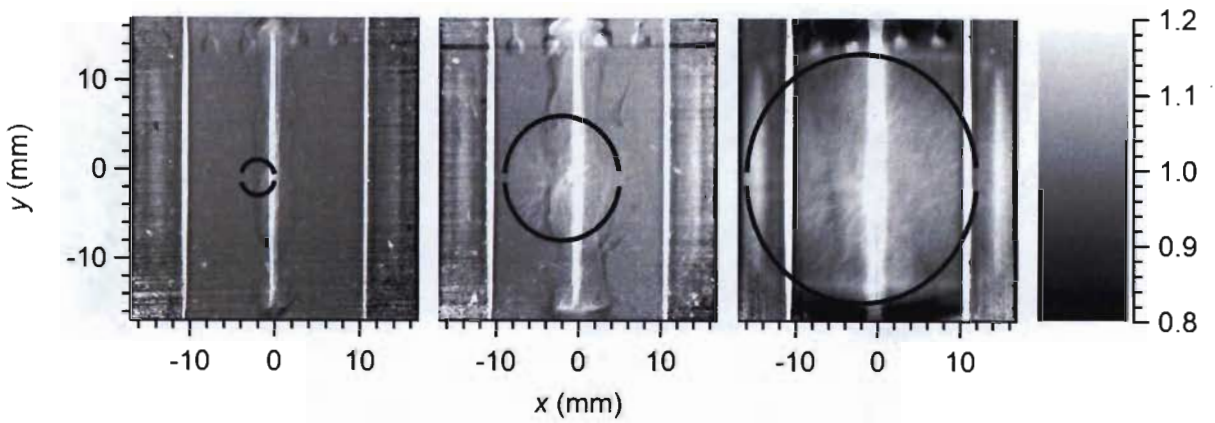

Figure 15: Smilowitz et al.

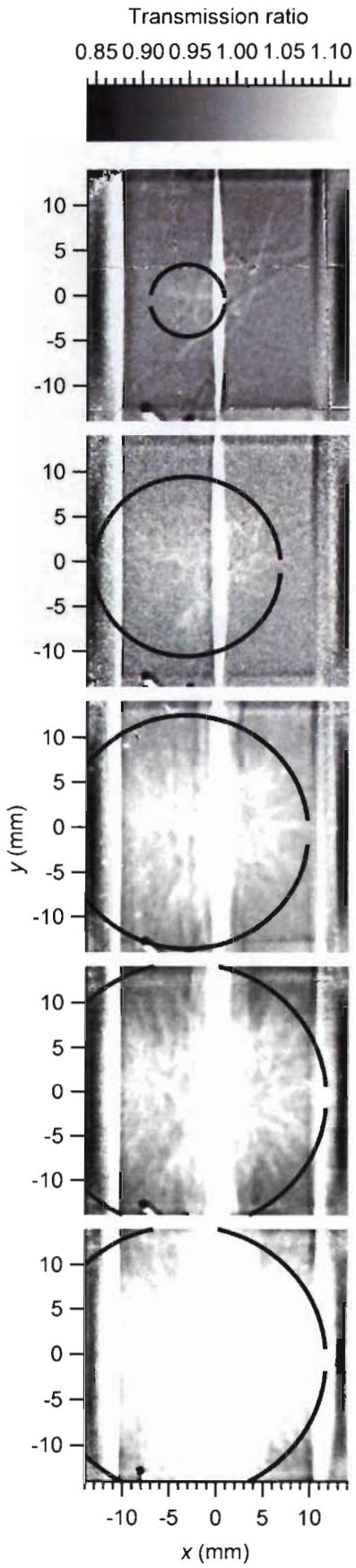

Figure 16: Smilowitz et al.